Section 2. Glass-ceramics and crystallization process

Crystallization mechanism and properties of a blast furnace slag glass

C. Fredericci [a], E.D. Zanotto [a,*], E.C. Ziemath [b]

[a] *Vitreous Materials Laboratory – LaMaV, Department of Materials Engineering – DEMa, Federal University of São Carlos, UFSCar, C.P. 676, 13565-905 São Carlos, SP, Brazil*
[b] *Department of Physics, IGCE – UNESP, C.P. 178, 13500-970 Rio Claro, SP, Brazil*

Abstract

The complex crystallization process of a Brazilian blast-furnace slag glass was investigated using differential scanning calorimetry (DSC), X-ray diffraction, optical microscopy, transmission electron microscopy (TEM), selected area diffraction (SAD), energy dispersive spectroscopy (EDS) and micro-Raman spectroscopy. Three crystalline phases (merwinite, melilite and larnite) were identified after heat treatment between T_g (742°C) and the DSC crystallization peak ($T = 1000$°C). Merwinite was identified as a metastable phase. A small amount (0.004 wt%) of metallic platinum was found in the glass composition. Particles of Pt_3Fe, detected by EDS and SAD–TEM, were the starting points of crystallization acting, therefore, as heterogeneous nucleating sites. Only melilite and larnite precipitated in a glass sample heat-treated at 1000°C for 1 h. The flexural strength of this crystallized sample was less than that of the glass, probably due the allotropic phase transformation of larnite. © 2000 Published by Elsevier Science B.V. All rights reserved.

1. Introduction

The volume of slag varies according to the raw materials used to produce pig iron; typically, 300 kg of blast-furnace slag are produced per ton of pig iron. The amount of this waste material produced at CSN (Companhia Siderúrgica Nacional, RJ, Brazil), for example, is approximately 1.2 million tons per year. The use of this material is an issue of ongoing concern for both economic and ecological reasons. Little effort has been made in Brazil so far to study the use of blast-furnace slags in glass–ceramics. Although the process to pro-

duce slag glass–ceramics has been known for a long time [1], the experiments described in the literature can only serve as a tentative guide for the study of different slags [2].

The vast quantity of blast-furnace slags produced in Brazil and the successful conversion of these materials into glass-ceramics in other countries [3,4] were the main reasons this study was undertaken. Properties such as high strength, hardness and wear resistance have allowed slag glass-ceramics to be used successfully in several applications, including the civil construction industry [5]. Obtaining glass-ceramics with improved properties for applications, depends not only on the ease with which the glass can be prepared and crystallized, but also on the microstructure and crystalline phases developed through heat treatment. Crystallization starting on the glass surface

---

* Corresponding author. Tel.: +55-16 274 8250; fax: +55-16 272 7404.

E-mail address: dedz@power.ufscar.br (E.D. Zanotto).

or from a small number of sites in the bulk usually results in low strength materials due to their coarse grained microstructures. On the other hand, efficient nucleation of crystals from numerous sites produces finer-grained microstructures and, consequently, greater strength materials. Normally, a nucleating agent must be added to the glass to promote controlled crystallization of a large number of microns or even nanometer-sized crystals. Among these, TiO_2, sulfides and Fe_2O_3 are particularly effective for slag glasses [6].

This paper considers the crystallization mechanism of an unaltered blast-furnace slag composition. We hope that, once the complex crystallization of this system is known, it will be possible to optimize the crystallization process through compositional adjustments and thermal treatments to obtain glass-ceramics with useful properties.

2. Experimental

2.1. Raw materials, melting and sample preparation

The process consisted of grinding a slag from CSN for 3 h to minimize its inhomogeneity, followed by dry magnetic separation of the metallic iron of the ground slag. The glass was prepared by melting the 'clean' slag in a platinum crucible at 1460°C for 3 h, followed by crushing and remelting it twice for 2 h to increase homogeneity. A Pt-crucible was chosen to minimize corrosion, whose products would change the slag glass composition. The liquid was quenched by pouring it onto a steel plate and then pressing it quickly with another stainless steel plate to suppress crystallization. Thermal treatments were performed in an electrical furnace having a thermal stability of ±2°C under various heating schedules. After polishing and etching, the samples were observed by optical microscopy and μ-Raman spectra were obtained from different regions. The chemical compositions of the slag and the glass were determined by inductively coupled plasma-atomic emission spectroscopy (ICP-AES-Thermal Jarrel Ash – model Atomscan 25). The results, shown in Table 1, were

Table 1
Chemical composition (wt%) of the slag (after magnetic separation) and investigated glass

Components	Slag	Glass
CaO	43.5 ± 0.5	43.7 ± 0.4
SiO_2	35.8 ± 0.4	35.5 ± 0.6
Al_2O_3	11.8 ± 0.2	11.5 ± 0.2
MgO	6.20 ± 0.1	6.0 ± 0.1
Fe_2O_3	0.3 ± 0.05	0.30 ± 0.03
TiO_2	0.8 ± 0.1	0.7 ± 0.1
MnO	0.7 ± 0.1	0.7 ± 0.1
P_2O_5	0.07 ± 0.03	0.04 ± 0.01
Na_2O	0.08 ± 0.01	0.07 ± 0.02
K_2O	0.50 ± 0.04	0.40 ± 0.04
S	0.80 ± 0.05	0.04 ± 0.01
C	0.40 ± 0.05	0.03 ± 0.003
Pt	–	0.004 ± 0.0002

evaluated from an average of two measurements for each sample.

2.2. Differential scanning calorimetry

Differential scanning calorimetric (DSC) measurements were performed (Netzsch DSC, Model 404), using a 20°C/min heating rate. Both fine (<74 μm) and coarse (177–297 μm) powdered glasses, weighing (20 ± 4) mg, were placed in a Pt pan, an empty Pt pan being used as a standard. Data were recorded using a computer-driven data acquisition system.

2.3. X-ray diffraction

To investigate the crystalline phases corresponding to the DSC thermogram peaks, the finely ground samples ($d < 74$ μm) were heat-treated at the temperatures corresponding to the exothermic peaks in the DSC curve at 20°C/min. When the chosen temperature was reached, the sample was removed immediately and allowed to cool to room temperature. The crystalline phases were identified in an X-ray powder diffractometer (Siemens 5000 D), using the copper K_α radiation ($\lambda = 15,418$ Å) and a nickel filter.

2.4. Optical microscopy

The number and size of crystals of the heat-treated samples were characterized by transmitted

light using a microscope (Jenapol–Carl Zeiss/ Jena). The thickness of the sample (about 0.8 mm) was measured by micrometer and a fixed area (0.8×0.5) mm^2 was selected in the microscope. The number of crystals per unit volume, N_v, was counted by shifting the focus from one surface to the other.

2.5. Transmission electron microscopy

Nucleation studies were made using a transmission electron microscope (TEM – BS 540 Tesla) with a 200 kV accelerating voltage. Mechanically thinned samples of crystallized glasses were dimple-ground, followed by ion-beam thinning to electron transparency for TEM analysis. The onset of crystal growth was determined through electron diffraction. The elemental composition of the particles present at the center of the crystals and the glass matrix were determined using an EDX Link system coupled to the electron microscope.

2.6. Micro-Raman spectroscopy

Identification of the crystalline phases in the bulk and on the crystallized surface layer was carried out by μ-Raman spectroscopy. Raman spectra were obtained with a Dilor XY spectrometer. The microscope lens used (Olympus, MS Plan, 100X, NA = 0.95) allows for the formation of a focal cylinder having an approximate diameter of 1.2 μm and a depth of around 2.5 μm. The focal cylinder was positioned on the crystal from which the spectrum would be obtained. The 514.5 nm (green) line of a Coherent Innova 70-2 Argon ion laser, with output power of about 100 mW exciting radiation, was used. An interference filter was used to avoid spurious scattered light from the laser plasma lines. The spectra were obtained in the backscattering geometry.

2.7. Flexural strength measurements

The flexural strength of the glass and glass-ceramics was measured using the room temperature 3-point test. Five measurements were taken for each sample, employing an Instron Machine, Model 1117, with a crosshead speed of 0.5 mm/ min.

2.8. Microhardness measurements

Vickers microhardness was measured (FM-Future Tech Corporation). The samples were indented with a 50 g load for 10 s. The data were evaluated from an average of 10 indentations for each sample.

2.9. Chemical durability

Grained glass and glass-ceramic samples, with sizes ranging from 0.4 to 0.5 mm, were used according to a standard procedure described in Ref. [7], in which about 2 g samples were heat-treated at 95°C for 1 h in a 0.01M HCl.

3. Results

3.1. DSC analysis

Samples having different specific surface area were studied by DSC to determine the crystallization mechanism (surface or volume crystallization) of the glass. Fig. 1 shows the curves for finely (<74 μm) and coarsely (177–297 μm) powdered glass. The related data are listed in Table 2. The glass-transition temperature, T_g, was determined as the point of intersection of the straight-lines extending from the tangents of the DSC curves in the region of the baseline shift. Some similar features of each thermogram are apparent: (a) a reversible endothermic peak at about 742°C, corresponding to the glass-transition temperature, T_g; (b) two exothermic events with maxima in the range of 920–1045°C, indicating crystallization, T_c; (c) two endothermic events at about 1280–1315°C, involving the melting of some crystal phases, T_m.

The increase in the specific area does not affect the glass-transition temperature, whereas the crystallization peak maxima shift towards lower temperatures with decreasing particle size. A difference of about 26°C between the crystallization
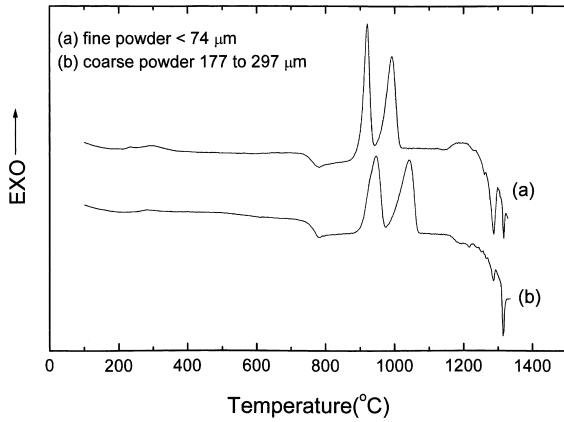
Fig. 1. DSC curves of the powdered glass samples. Heating rate: 20°C/min.

Fig. 2. X-ray patterns of the powdered sample heat-treated at: (a) 1000°C; (b) 926°C.

of the coarse and fine powders was observed for the first crystallization peak.

3.2. Crystalline phases

The exothermic peaks in the DSC curves were identified using XRD diffraction patterns. Finely powdered samples (<74 μm) were heat-treated at temperatures corresponding to the maximum peak temperature of the DSC curves, i.e., 920°C and 1000°C, respectively.

Fig. 2(a) shows that the first crystalline phase is merwinite. Two crystalline phases can be observed in Fig. 2(b), i.e., melilite and larnite (as a minor phase) but no merwinite. These results indicated that the first peak observed in the DSC curve is associated with the crystallization of a metastable phase, namely, merwinite.

According to Kalinina and Filipovich [8], metastable crystalline phases commonly precipitate in multicomponent glasses at the initial stages of low temperature ($\sim T_g$) crystallization. Upon
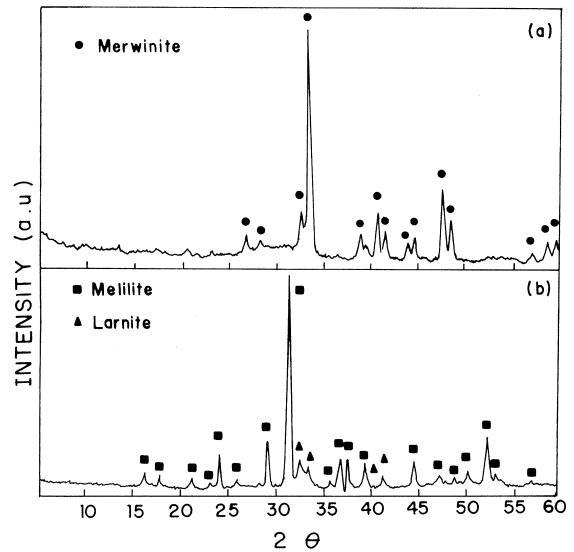
further heating, these metastable phases irreversibly disappear by becoming transformed into the thermodynamically stable phase corresponding to the phase diagram of the system. The major constituents of the slag glass are CaO, SiO_2, Al_2O_3 and MgO and its composition lies around the 10% Al_2O_3 of the $CaO–SiO_2–Al_2O_3–MgO$ system (Fig. 3) which corresponds to the primary field of melilite. A probable interpretation of the formation of larnite (Ca_2SiO_4) is that the slag composition has more SiO_2 and CaO than is necessary to form $2CaO·MgO·2SiO_2$ (akermanite) and $2CaO·Al_2O_3·SiO_2$ (gehlenite), a series known as melilite. The excess of CaO and SiO_2 are then sufficient to form a calcium silicate.

As-quenched glass samples heat-treated at 893°C for 2 h (i.e. between T_g and T_c) showed radially distributed needle-like crystals forming

Table 2
DCS analysis, where T_g is the glass-transition temperature, T_{c1} and T_{c2} the maxima crystallization peak temperatures, T_{m1} and T_{m2} are the melting points of crystalline phases[a]

Particle size (μm)	T_g (°C)	T_{c1}(°C)	T_{c2}(°C)	T_{m1}(°C)	T_{m2}(°C)
<74	742	920	1000	1285	1315
177–297	742	946	1044	1285	1315

[a] The estimated error is about 2°C.

spherulitic crystals and a crystalline surface layer (Fig. 4). Fig. 5 shows the micro-Raman spectra obtained from the glass matrix, from the spheru-
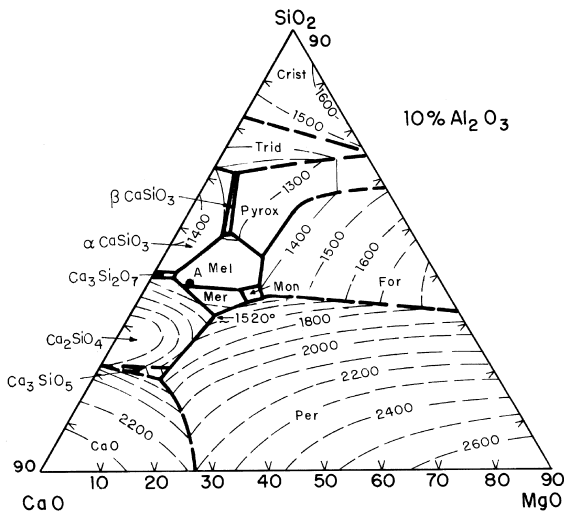

Fig. 3. Phase Diagram of the CaO–SiO$_2$–Al$_2$O$_3$–MgO system with 10 wt% Al$_2$O$_3$ [9]. Point A gives an approximate indication of the composition of the glass.

litic crystal, and the crystalline surface layer. A spectrum of a natural merwinite from Bulgaria is also presented in Fig. 5 to facilitate the interpretation of the results. The Raman spectrum of merwinite is consistent with that obtained by Piriou and MacMillan [10]. The bands at 852 and 817 cm^{-1} correspond to the modes derived from symmetric v_1 and asymmetric v_3 stretching vibrations of the SiO$_4$ tetrahedra of the monticellite [10]. This phase was defined by XRD to be an impurity in the natural merwinite.

A band at 880 cm^{-1} in the Raman spectrum of the glass is observed in Fig. 5(a). This peak is attributed to the presence of an appreciable number of non-bridging SiO$_4^{4-}$ groups in the glass network [11]. Piriou and McMillan [10] studied the vibrational spectra of vitreous CaMgSiO$_4$ and suggested that part of the bands at 530 and 580 cm^{-1} might be due to MgO vibrations; however, their assumption was not confirmed. A comparison of the 5b, 5c, and 5d spectra reveals that the crystalline phase, which forms the spherulite, and the crystalline layer is merwinite. Although, the bands
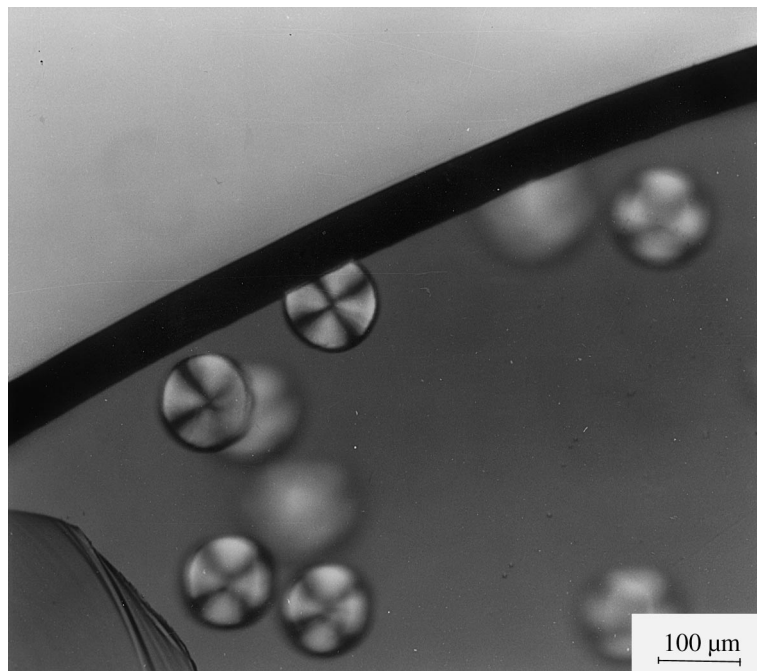

Fig. 4. Optical micrograph of the slag glass sample heat-treated at 893°C for 30 min.

of the crystal precipitated from the glass are smaller and wider than that of the mineral, their maxima match closely. In Raman spectroscopy, the width of the bands is determined by structural ordering of the material. The broader bands of the crystals in the glass compared to the bands of the mineral indicate some disorder at Si or Al sites. This feature may be related to the residual glass
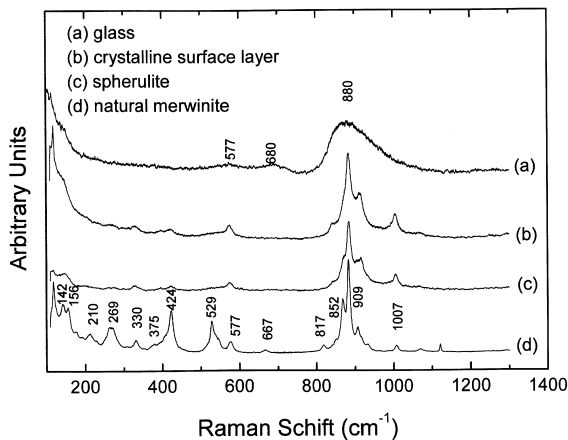

Fig. 5. Raman microprobe spectra of: (a) slag glass; (b), (c) crystalline surface layer and spherulitic crystal, respectively, shown in Fig. 4; (d) natural merwinite.

between the radially distributed needles forming the spherulitic crystal.

Orsini et al. [12] studied glass crystallization in the akermanite–gehlenite system ($2CaO \cdot (1-x)MgO \cdot xAl_2O_3 \cdot (2-x)SiO_2$) and found merwinite as a metastable phase when $x \leqslant 0.6$. They report that glasses with melilite compositions are considered to be inverted glasses due the large number of modifying oxides and have a very fragmented lattice, stabilized by ionic bonds between the modifying cations and simple SiO_4^{4-} units. It was suggested that, in glasses with $x < 0.6$, the fraction of simple tetrahedra and the MgO concentration were sufficient to form merwinite ($Ca_3Mg(SiO_4)_2$).

The crystallization of merwinite causes exsolution of Al^{3+}, resulting in a glass rich in Al_2O_3 between the merwinite needles that is probably more viscous than the original glass. For the formation of melilite, therefore, longer times and higher temperatures would be necessary for the AlO_4 tetrahedra diffusion, since the melilite structure consists of MgO_4, SiO_4 and AlO_4 tetrahedra sheets [13].

Fig. 6 shows an optical micrograph of a sample heat-treated at 893°C for 22 h. It is possible that the spherulite undergoes a phase transformation
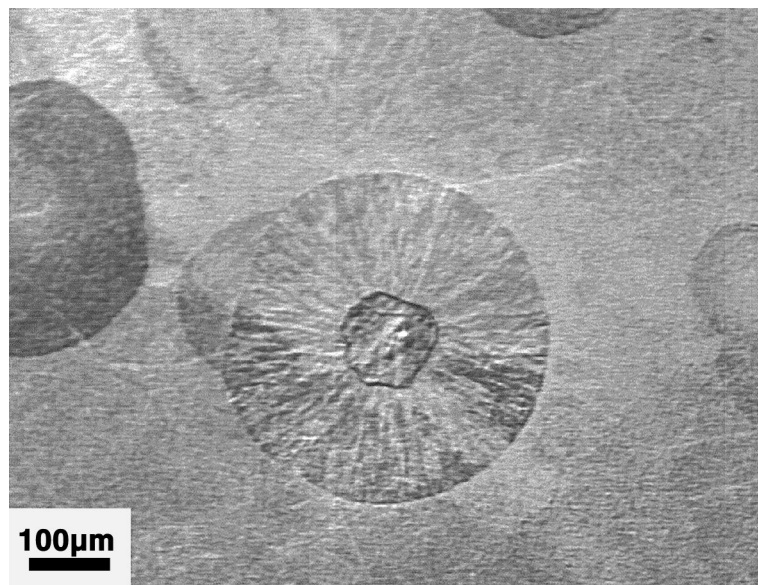

Fig. 6. Optical micrograph of the slag glass sample heat-treated at 893°C for 22 h.

starting at its center. Raman microprobe spectra measurements were taken on the spherulitic crystal in this region (Fig. 7). Since no Raman spectrum of melilite was found in the literature, a pattern of one natural melilite from Russia was reproduced and is also shown in Fig. 7. As mentioned earlier, melilite is a solid solution between akermanite and gehlenite. The Raman spectra of the both crystalline phases can be found in Refs. [11,14], respectively. The melilite spectrum is not exactly a sum of these spectra. The absence of some characteristic crystalline gehlenite and akermanite bands in the melilite spectrum can be explained by modifications of the interatomic distances and bond angles in the melilite solid solution, making some Raman vibrational modes inactive. However, the strongest gehlenite band, at 626 cm^{-1}, corresponding to asymmetrical stretching mode (v_s (T–O–T), where T = Al or Si) of the bridging oxygen and the strongest akermanite band at 661 cm^{-1} corresponding to the v_s (Si–O–Si) can be found in the melilite spectrum.

Other aspects of Fig. 7(a) that require discussion are the presence of a band at 973 cm^{-1}, which was not observed in the spectrum of the natural melilite, and the high intensity of the bands at 855 and 842 cm^{-1} in relation to those found in the melilite pattern. Reynard et al. [15] studied the high-pressure transformation of larnite. They report a Raman spectrum of larnite that corresponds

to a partial transformation of β-Ca$_2$SiO$_4$ to γ-Ca$_2$SiO$_4$. Bands at 973, 855 and 842 cm^{-1} were found in this spectrum that coincide with those found in this work. It is known that larnite crystallizes as the α- or β-phase at high temperatures and that the β-phase inverts to γ-phase at 675°C with increased volume [16]. The sample used for the Raman spectroscopy study was heat-treated at 893°C for 22 h, removed from the furnace and cooled in air. It is possible that cooling occurred fast enough to avoid completion of phase transformation.

A comparison of the spectra reveals that the crystalline phases developed in the center of the spherulites were melilite and larnite, while the phase corresponding to spherulitic crystals is merwinite. These data confirm that merwinite is a metastable phase in this system and are consistent with those found by XRD.

3.3. Kinetics of nucleation

As-quenched glass samples were heat-treated at 750°C, 770°C and 790°C for 2, 4, 6 and 8 h for nucleation, followed by heat treatment at 893°C for 30 min for crystal growth. The samples were polished and the number of crystals per unit volume determined, as described in Section 2.4.

Fig. 8 shows the numbers of crystals versus time of heat treatment of the glass samples at different temperatures. The related data are shown in Table 3. There is a statistical scatter around a mean $N_v \sim 13$ crystals/mm^3 and N_v does not depend on the heat treatment time, indicating that crystallization occurs from a fixed number of sites. This result is typical of heterogeneous nucleation.

3.4. Nucleation mechanism

The TEM micrograph of a sample heat treated at 873°C for 10 min, used in the crystal growth study, shows a particle in the crystal center (Fig. 9). This particle was identified as Pt$_3$Fe by EDS and selected area diffraction (SAD-TEM). Fig. 10(c) shows the EDS spectra of the central particle and of the crystalline phase. Although the slag composition contains iron, this particle contained larger amounts of Fe as well as Pt that was not
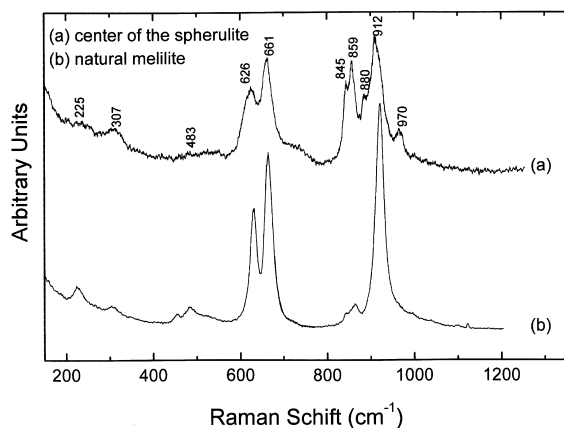

Fig. 7. Raman microprobe spectra of: (a) center of the spherulitic crystal shown in Fig. 6; (b) natural melilite.
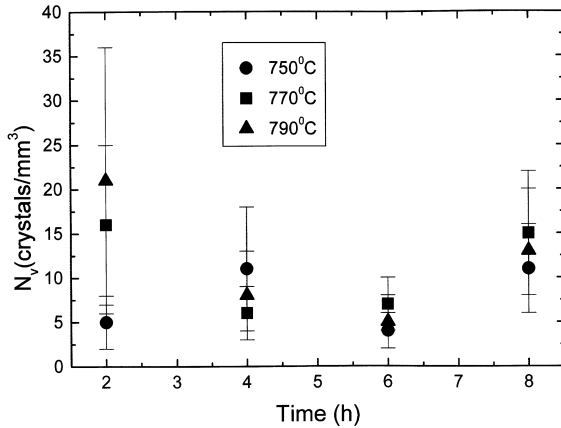
Fig. 8. Average number of merwinite crystals per mm^3 on the slag glass sample after heat treatment at different times and temperatures.

Table 3
Number of crystals per unit volume (N_v) for different thermal treatments

Temperature (°C)	Time (h)	N_v (crystals per mm^3)
750	2	5 ± 3
	4	11 ± 7
	6	4 ± 2
	8	11 ± 5
770	2	16 ± 9
	4	6 ± 3
	6	7 ± 3
	8	15 ± 7
790	2	21 ± 15
	4	8 ± 5
	6	5 ± 3
	8	13 ± 7

observed in the EDS spectrum of the crystalline phase. Indexing of the electron diffraction pattern, described by Beenston et al. [17], was compared with a simulation performed by our software. Table 4 shows the comparison of d-spacings of Pt$_3$Fe from JCPDS with that obtained from ED in this work. The d-spacings match. Hence, the Pt$_3$Fe particles were assumed to act as a heterogeneous nucleating agent in the crystallization of the glass. It is known that platinum and iron form alloys at high temperature [18] and, despite our efforts to eliminate the slag's iron prior to melting, some metallic iron remained in our samples.

Table 4
XRD and ED data of Pt$_3$Fe from the slag glass

JCPDS (29–716)		This work
hkl	d (Å)	d (Å)
111	2.23	2.23
311	1.16	1.12
200	1.93	1.90
400	0.97	0.93

3.5. Crystal growth

Fig. 10 shows merwinite growth velocity, U, determined by measuring the largest diameter of the spherulites as a function of time and temperature. At large undercoolings, below the maxima of growth rates, crystal growth velocity can be written as $U = f a_0 v \exp(-\Delta G_D / RT)$, where ΔG_D is the activation energy for diffusion across the boundary, f the fraction of sites of the crystal surface available for attachment, a_0 the thickness per molecular layer, v the vibrational frequency, R the gas constant, T is the absolute temperature. Neglecting pressure effects, $\Delta G_D = \Delta H_D T \Delta S_D$ and expressing $A = f a_0 v \exp(\Delta S_D / R)$, the equation of crystal growth rate can be written as: $U \approx A \exp(-\Delta H_D / RT)$, where ΔH_D is the activation enthalpy for crystal growth [19]. A plot of ln U versus $1/T$, in these conditions, should yield a straight line with slope proportional to ΔH_D. We determined from Fig. 11 that the activation energy for merwinite growth is 150 kJ/mol. Orsini et al. [12] determined the activation energy for merwinite growth, by a DTA method, as being 165 kcal/mol in a glass with composition $2CaO \cdot (1-x)MgO \cdot xAl_2O_3 (2-x)SiO_2$, where $0 \leqslant x \leqslant 1$.

3.6. Mechanical and chemical properties

Flexural strength, Vickers hardness and chemical durability were investigated to determine other properties of the resulting glass-ceramic. The results for the glass and a glass-ceramic sample heat treated at 1000°C for 1 h are given in Table 5. XRD diffraction data showed that the crystalline phases were melilite and larnite. Crystallization yielded a material having a smaller flexural strength than that of the glass samples. Larnite
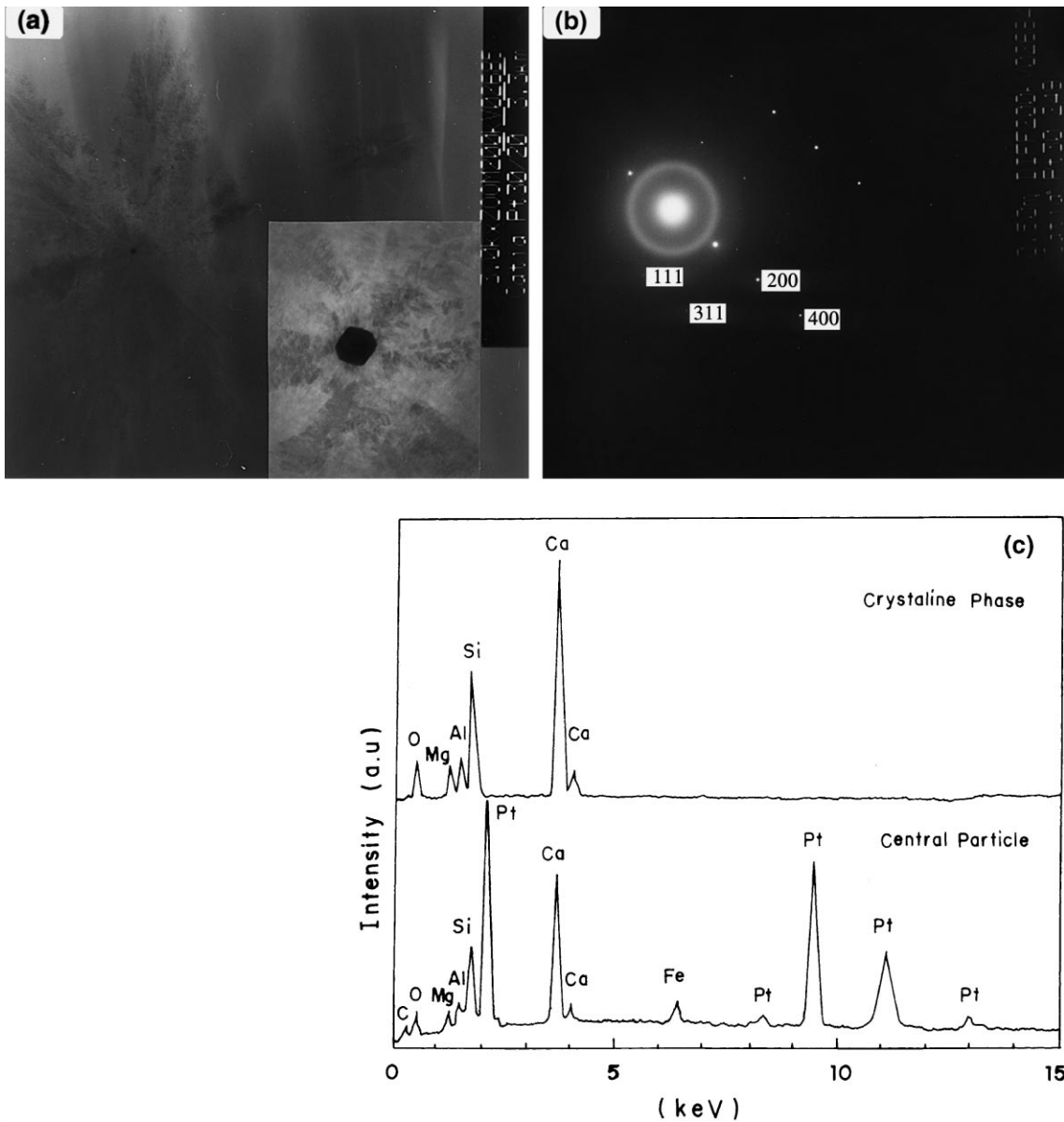
Fig. 9. (a) TEM photomicrograph, inserted: enlarged view of the central particle. (b) ED pattern of the sample heat-treated at 873°C for 10 min. (c) EDS spectra of the central particle and crystalline phase.

undergoes a phase change and the volume increase accompanying this transformation caused cracking in the bulk of the glass-ceramic samples, which decreased its strength.

Table 5 shows the indentation hardness of the glass and its corresponding glass-ceramic. It can

be noted that hardness is not substantially increased. Agarwal et al. [20] found Vickers microhardness values as large as 9 GPa for a glass deriving from cupola slag glass, in which the predominant crystalline phase was Mg-wollastonite.
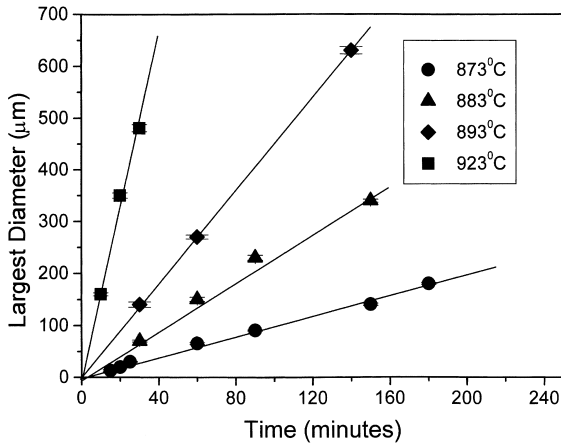
Fig. 10. Largest merwinite crystal diameter in the volume of the slag glass at 873°C, 883°C, 893°C, 923°C.

Fig. 11. Ln U versus $1/T$.

The results of the chemical durability test of the glass and glass-ceramic are also shown in Table 5. The method used in this work was the same as that used by Karamanov et al. [7] with the purpose of comparing the results, particularly as they studied glass-ceramics from waste raw materials. They found 0.3 wt% loss for one glass-ceramic, in which the major crystalline phase was diopside and a 1.4 wt% loss from a glass-ceramic containing wollastonite as the principal phase. They reported that the chemical durability of these materials is high. Kruchnin [21] reported that melilite glass-ceramics are highly acid resistant. In this research work, values of about 1.2 wt% loss for the glass and glass-ceramic containing melilite and larnite were found.

4. Discussion of nucleation mechanism

In the DSC curve (Fig. 1) a difference of about 26°C between the crystallization of the coarse and fine powders was observed for the first crystallization peak. According to Takur [22], in the case of high-catalyzed volume crystallization of glass, the difference between the exothermic peak temperature of a coarse and fine particle should be small or, ideally, nil. Hence, the shift of the exother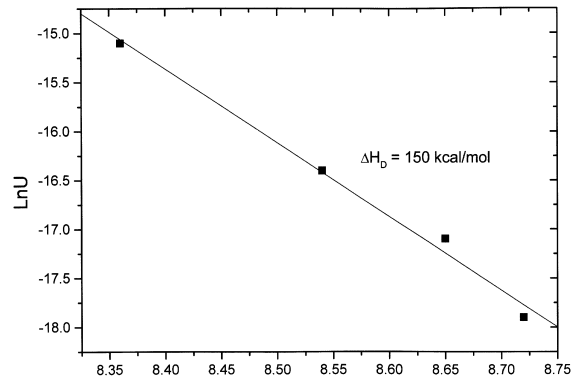mic peak to a lower temperature with the decrease of the glass particle size suggests that crystallization occurs essentially on the surface and that volume crystallization is either low or absent. This was confirmed in the nucleation kinetics study (Section 3.3) since the numbers of crystals per unit volume N_v lay around 13 crystals per mm^3.

An optical micrograph of one glass sample heat treated at 893°C for 30 min shows a spherulitic crystal and the crystalline surface layer (Fig. 4). The number of crystals was so small that spherulites as large as 480 μm could be observed after heat treatment at 923°C for 30 min (Fig. 12). Therefore, the results of the kinetics study are in agreement with those of DSC.

TEM study of heat-treated glass samples showed the presence of Pt_3Fe particles considered to act as heterogeneous nucleating agent. Agarwal et al. [23] studied the crystallization of a cupola slag glass with the following approximate composition: 42% SiO_2, 34% CaO, 11% MgO, 8%

Table 5
Glass and glass-ceramic properties

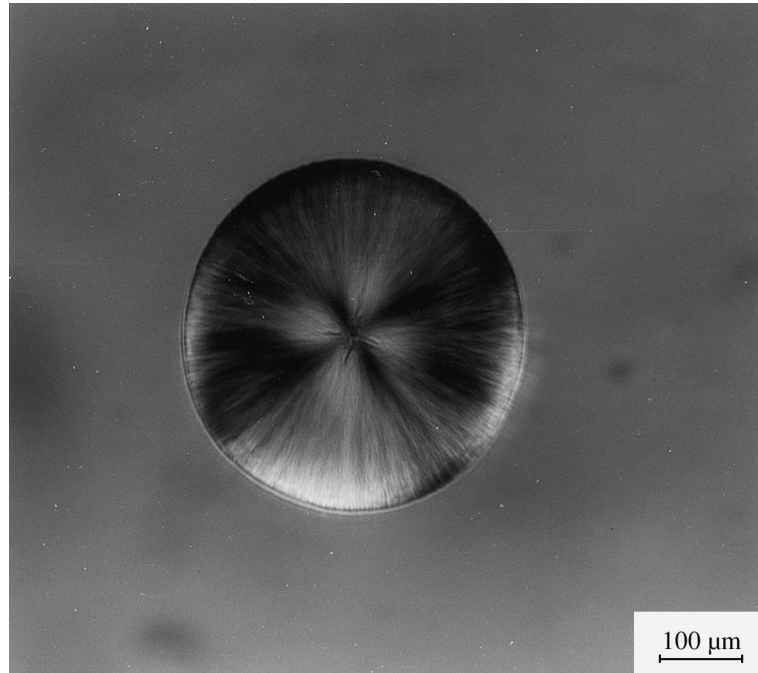| Properties	Glass	Glass-Ceramic
Flexural strength (MPa)	100 ± 20	69 ± 9
Vickers hardness (GPa)	5.2 ± 0.4	5.5 ± 0.1
Chemical resistance (wt% loss in 0.01M HCl)	1.2 ± 0.1	1.3 ± 0.05

Fig. 12. Optical micrograph of the slag glass sample heat-treated at 923°C for 30 min.

Al_2O_3, 3% MnO and impurities such as iron oxide, titanium oxide, sulfur oxides, etc. They found, by TEM, that the as-quenched glass contained iron, manganese and sulfur droplets and suggested that complex-wollastonite crystals grew from them. These kinds of particles were not found in our samples.

5. Conclusions

This study shows that the blast-furnace slag from CSN can be melted and formed into a glass, undergoing both surface and volume crystallization upon heating. However, internal crystallization is only possible due the formation of Pt_3Fe during melting in a Pt crucible. Melilite was the predominant phase, with a small content of larnite and merwinite, which was demonstrated to be metastable. Based on the variation in the DSC peak temperature, monitored as a function of the particle size of the glass, we suggested that most crystallization was on surfaces. This suggestion was confirmed by the study of nucleation kinetics.

It is possible to produce glass-ceramics with this slag. However, owing to the phase transformation of larnite, the flexural strength is inferior to that obtained for glass-ceramics used in the civil construction industry. Further work is required to improve the properties of these glass-ceramics.

References

[1] I.I. Kitaigoroskii, M.N. Pavluskin, S.V. Petrov, Inorg. Mater. 2 (1966) 323.

[2] M.W. Davies, B. Kerrison, W.E. Gross, M.J. Robson, D.F. Wichall, J. Iron Steel Instrum. 208 (1970) 348.

[3] T. Shaoqiu, L. Zhongjun, C. Guorong, J. Am. Ceram. Soc. 75 (1992) 440.

[4] M.C. Wang, M.H. Hon, J. Ceram. Soc. Japan 98 (1990) 625.

[5] L.J. Shelestak, R.A. Chavez, J.D. Mackenzie, B. Dunn, J. Non-Cryst. Solids 27 (1978) 83.

[6] N.M. Pavluskin-Vitrokeramik, Grundlagen der Technologie, VEB Deutscher Verlag für Grundstoffindustrie, Leipzig, 1984.

[7] A. Karamanov, I. Gutzow, I. Penkov, J. Andreev, B. Bogdanov, Glastech. Ber. – Glass Sci. Technol. 67 (1994) 202.

[8] A.M. Kalinina, V.N. Filipovich, Glass Phys. Chem. 21 (1995) 97.

[9] E.M. Levin, C.R. Robbins, H.F. McMurdie, Am. Ceram. Soc. 2 (1969) 185.

[10] B. Piriou, P. McMillan, Am. Mineral. 68 (1983) 426.

[11] S.K. Sharma, H.S. Yoder Jr., Carnegie Inst. Washington, Yearb. 78 (1979) 526.

[12] P.G. Orsini, A. Buri, A. Marotta, J. Am. Ceram. Soc. 58 (1975) 306.

[13] Th.G. Sahama, M. Lehtinen, C. R. Soc. Géol. Finlande 39 (1967) 29.

[14] S.K. Sharma, B. Simons, H.S. Yoder Jr., Am. Mineral. 68 (1983) 1113.

[15] B. Reynard, C. Remy, F. Takir, Phys. Chem. Miner. 24 (1997) 77.

[16] J. Phemister, Mineral. Mag. 26 (1942) 225.

[17] B.E.P. Beenston, R.W. Horne, R. Markhan, in: Audray M. Glauert (Ed.), Practical Methodes in Electron Microscopy, North-Holland, Amsterdam, 1972, p. 444.

[18] R. Hultgren, Selected Values of the Thermodynamic Properties of Binary Alloys, American Society for Metals, Metals Park, OH, 1973, pp. 861–865.

[19] E.D. Zanotto, PhD thesis, Sheffield University, 1982.

[20] G. Agarwal, R.F. Speyer, J. Non-Cryst. Solids 135 (1991) 95.

[21] Y.D. Kruchnin, Inorg. Mater. 9 (1966) 1441.

[22] R.L. Thakur, Determining the suitability of nucleating agents for glass-ceramics, Adv. Nucl. Cryst. Glass, special edition, 5 (1971) 166.

[23] G. Agarwal, K.S. Hong, M.R. Fletcher, R.F. Speyer, J. Non-Cryst. Solids 130 (1991) 187.